

Article

Dynamic Matching of Reconstruction and Anti-Aliasing Filters in Adaptive Active Noise Control

Fangjie Zhang ^{1,2,*}, Yanqin Wu ^{1,2}, Yifan Wang ^{1,2} and Xiaodong Li ^{1,2} 

¹ Key Laboratory of Noise and Vibration Research, Institute of Acoustics, Chinese Academy of Sciences, No. 21 North 4th Ring Road, Haidian District, Beijing 100190, China; wuyanqin@mail.ioa.ac.cn (Y.W.); wangyifan@mail.ioa.ac.cn (Y.W.); lxd@mail.ioa.ac.cn (X.L.)

² University of Chinese Academy of Sciences, No. 19(A) Yuquan Road, Shijingshan District, Beijing 100049, China

* Correspondence: zhangfangjie@mail.ioa.ac.cn

Abstract: Constrained by the computing power, adaptive active noise control systems often have a low sampling rate. Therefore, reconstruction filters and anti-aliasing filters with fixed parameters are generally adopted to eliminate the mirror noise and aliasing noise, respectively; however, they may boost the group delay of the system. A dynamic matching method based on dual sampling rates is proposed to dynamically adjust the parameters of the reconstruction and anti-aliasing filters, according to the characteristics of the primary sound source, for a compromise between high-frequency noise and group delay. In digital high-sampling-rate regions, data that include high-frequency information are analyzed regularly, following which the parameters of the reconstruction filters and those of the anti-aliasing filters are dynamically matched. In digital low-sampling-rate regions, the estimation of the secondary path transfer function is updated. The results of laboratory experiments show that the proposed method not only can suppress the mirror and aliasing noise for primary sound sources with different spectra, but can also effectively reduce the group delay and improve the noise reduction performance of a system.

Keywords: active noise control; anti-aliasing filter; multi-rate system; reconstruction filter



Citation: Zhang, F.; Wu, Y.; Wang, Y.; Li, X. Dynamic Matching of Reconstruction and Anti-Aliasing Filters in Adaptive Active Noise Control. *Appl. Sci.* **2024**, *14*, 4810. <https://doi.org/10.3390/app14114810>

Academic Editor: John S. Allen

Received: 28 March 2024

Revised: 30 May 2024

Accepted: 31 May 2024

Published: 2 June 2024



Copyright: © 2024 by the authors. Licensee MDPI, Basel, Switzerland. This article is an open access article distributed under the terms and conditions of the Creative Commons Attribution (CC BY) license (<https://creativecommons.org/licenses/by/4.0/>).

1. Introduction

Noise control methods can be divided into two main categories: passive noise control and active noise control (ANC) [1]. Passive noise control methods can be used to effectively suppress middle- and high-frequency noise but hardly reduce low-frequency noise. Meanwhile, ANC technology offers an effective means of low-frequency noise control, and has been widely applied in active headphones and headrests, as well as in noise reduction for ventilation ducts [2]. The application of ANC technology in headphones is the most mature; however, wearing headphones may introduce ear-blocking effects, making users feel uncomfortable and causing interference in their actions or communications [3]. Hence, the local active noise control technology represented by active noise reduction headrests is flourishing. It has also found applications in scenarios such as automotive road noise control and aircraft cabin noise control, and related research is constantly being deepened [4–7].

Active noise control can be conducted with fixed coefficient methods and adaptive methods [1,8]. Fixed coefficient methods typically used in ANC headphones have a simple calculation process; thus, they can be applied for real-time control at high sampling rates [9,10]. Adaptive methods have significant advantages in tracking changes in the sound field environment, and are widely used in active headrests; however, their computational complexity may be much higher. Improving the sampling rate of a system helps to accelerate its response speed, but this poses significant challenges related to the real-time

computing performance and data throughput of the processor [10,11]. Therefore, researching methods for improving the noise reduction ability without increasing the requirements of computational performance is important.

At the algorithmic level, the FxLMS and NFxLMS algorithms are the two most basic types of algorithms used in the field of adaptive active noise control [12]. In addition, modified methods such as frequency-domain adaptive algorithms, multi-subband filtering algorithms, and delay-free subband filtering algorithms have emerged one after another [11,13]. As the partitioned block frequency-domain method uses different filter lengths to control noise at different frequencies, the computational requirements are further deducted in the low-frequency control process of these optimization algorithms [14]. These optimization algorithms successfully accelerate the convergence speed of ANC systems, improve their robustness, and reduce their computational requirements.

As the research deepens, the impact of the group delay introduced by hardware systems and algorithms in the control process has received much attention. Nelson et al. first emphasized the importance of causal constraints on the active control of sound [15]. Elliott et al. conducted an in-depth analysis of the group delay effect [1] and further studied the frequency-domain adaptation of causal digital filters [16]. With the increase in local active noise control systems in practical application scenarios, more discussions about group delay and causality have been conducted [17–19]. In order to avoid the limitations imposed by the spatial distance on the group delay, Shen et al. proposed an increase in the distance between the reference microphone and the error microphone using wireless transmission [20]. However, this method does not allow for long-frame caching and has extremely demanding delay requirements for the wireless transmission system. At the system level, the aliasing noise, mirror noise, and group delay introduced by control circuits have gradually received attention [21–23]. The aliasing noise represents the noise in the low-frequency band introduced by the high-frequency component in the extraction process, and the mirror noise represents the high-frequency noise correlated with the low-frequency signal in the interpolation or reconstruction process. To reduce the electronic delay of a single-rate ANC system, Bai et al. first systematically analyzed the group delay of single-rate systems and proposed a multi-rate signal-processing approach [24] that uses asymmetric FIR filters. However, this method requires a determined model to design the reconstruction filter and anti-aliasing filter under the assumption that the spectral structure of the primary sound source is known. As audio processing in ANC systems is an important application and the basic requirement of the sampling rate for audio processing is higher than that for active noise control, a multi-rate system has also been used to balance the computational complexity and functional requirements [25]. As field-programmable gate array (FPGA) processors develop, their better parallel calculation properties can significantly enhance the calculation speed; therefore, some researchers have tried to use FPGAs for room noise control [26] and head-mounted feedforward ANC systems [27]. The use of FPGAs is an effective way to enhance the processing speed, but the associated programming process is often difficult and inflexible, and the debugging work in such systems is tedious. Some other meaningful works have also been conducted [2], and another effective method is the use of parallel analog and digital adaptive feedforward controllers in a system [28]; however, accurately modifying the analog filter coefficient is often not easy. As the new proposed methods are often restricted by system flexibility and adjustment accuracy, Bai's method is still very attractive. According to the available literature, whether it is a single-rate system or a multi-rate system, the design of reconstruction and anti-aliasing filters is completed before the control starts, and the filter parameters remain fixed and unchanged in the control process [29–32]. In practical applications of adaptive ANC systems, the characteristics of the primary source may change over time, and the requirements for reconstruction and anti-aliasing filters also change. However, there is currently no in-depth research on the methods and effects of the dynamic matching of reconstruction and anti-aliasing filters.

In order for an adaptive ANC system to match the characteristics of a primary sound source in the control process, a dynamic matching method is proposed for the design of reconstruction and anti-aliasing filters. The core idea of this method is to replace the fixed parameters of model-based reconstruction and anti-aliasing filters with dynamic variations in these parameters driven by the data features. The remainder of this article is organized as follows. Section 2 outlines the traditional ANC systems and the challenges confronting them. Section 3 demonstrates the proposed dynamic matching method for reconstruction and anti-aliasing filters in adaptive noise control. Section 4 introduces the experimental setup and the results of the proposed method. Section 5 summarizes some important conclusions.

2. Background and Limitations: Conventional Methods

Single-rate systems and multi-rate systems are two commonly used kinds of traditional ANC systems [1,33]. In a single-rate system, the reconstruction filter and anti-aliasing filter are implemented with analog circuits that are typically composed of capacitors, inductors, resistors, and operational amplifiers. The transfer functions in acoustic regions from the primary source to the reference microphone and error microphone are denoted by $F_p(s)$ and $P_p(s)$, respectively. The principles of a single-channel multi-rate ANC system are shown in Figure 1. The primary sound source $v_p(t)$ reaches the reference microphone and error microphone after passing through $F_p(s)$ and $P_p(s)$, respectively, and the corresponding signals are $x_p(t)$ and $d_p(t)$, respectively. $d_p(t)$ is the noise reduction target of ANC, and $u_p(t)$ is the control signal given by the speaker. After passing through the secondary path of the sound field $G_p(s)$, the signal from the error microphone is $y_p(t)$. The transfer functions of the analog anti-aliasing filters are denoted by $T_{xa}(s)$ and $T_{ea}(s)$, and the transfer function of the analog reconstruction filter is denoted by $T_{ua}(s)$.

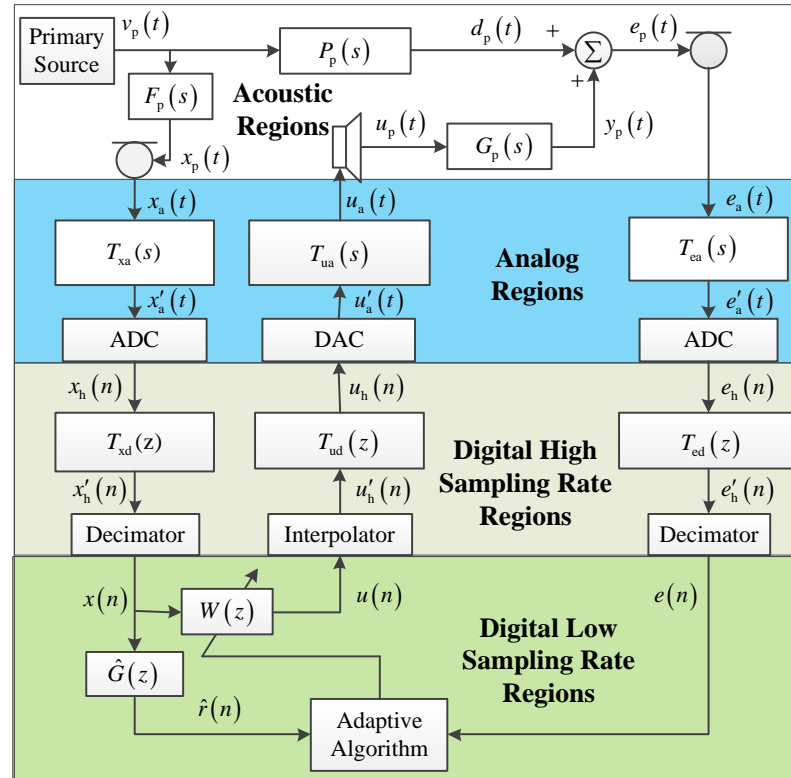


Figure 1. Conventional multi-rate ANC systems consist of four regions.

Compared with single-rate systems, a multi-rate system has additional digital regions with a high sampling rate. $T_{xd}(z)$ and $T_{ed}(z)$ correspond to digital anti-aliasing filters, and $T_{ud}(z)$ corresponds to a digital reconstruction filter. The reference signal and error signal

in the regions with the high sampling rate are denoted by $x_h(n)$ and $e_h(n)$, respectively. According to the FxLMS algorithm, the output signal of the digital control system is

$$u(n) = \mathbf{w}^T(n)\mathbf{x}_c(n) \tag{1}$$

where $\mathbf{w}(n) = [w_0(n) \ w_1(n) \ \dots \ w_{I-1}(n)]^T$ denotes a column vector composed of a number of coefficients at time n , and $\mathbf{x}_c(n) = [x(n) \ x(n-1) \ \dots \ x(n-I+1)]^T$. The adaptive filter coefficients are updated with

$$\mathbf{w}(n+1) = \mathbf{w}(n) - \mu \hat{\mathbf{r}}^T(n)e(n) \tag{2}$$

where μ denotes the update step size, $G(z)$ denotes the true transfer function from $u(n)$ through the loudspeaker to $e(n)$, and $\hat{G}(z)$ is the estimate of $G(z)$. The filtered reference vector $\hat{\mathbf{r}}(n) = [\hat{r}(n) \ \hat{r}(n-1) \ \dots \ \hat{r}(n-I+1)]^T$, where $\hat{r}(n)$ denotes the digital signal obtained by filtering the reference signal $x(n)$ with $\hat{G}(z)$.

Regardless of whether a single-rate or multi-rate active noise control system is considered, reconstruction and anti-aliasing filters are placed before the ANC block in current systems, and the filter parameters remain fixed during the control process. These preset filters are generally determined based on specific models that only consider their attenuation characteristics, and, so, mismatches may occur when the signal features change. The roll-off rate describes how rapidly the filter attenuates the signal after the cut-off frequency and is typically measured in decibels per octave (dB/octave) or decibels per decade (dB/decade). If the roll-off rate of the designed filter is insufficient, excessive mirror noise or reconstruction noise may be introduced into the system; on the contrary, if the roll-off rate of the designed filter is too fast, excessive group delay may be introduced by the filter, and the control system may not meet the causal requirements, leading to decreased controller performance or even system failure [1].

3. An Active Noise Control System with Dynamically Adapted Reconstruction and Anti-Aliasing Filters

This study proposes a method for the dynamic matching of reconstruction and anti-aliasing filters with fixed parameters in an ANC system for primary sound sources with different spectral structures. The designed filters have minimal system group delay, while the aliasing noise is suppressed to meet the dynamic range requirement of $x(n)$ and $e(n)$, as shown in Figure 1, and the mirror noise is reduced to less than a preset level in comparison with the original low frequency of $u(n)$. A schematic diagram of this method is shown in Figure 2.

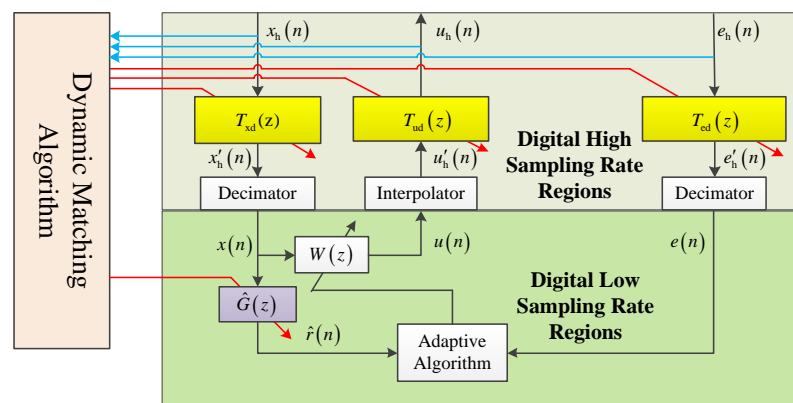


Figure 2. Schematic diagram of the proposed method including dynamic matching algorithm.

On the basis of a traditional multi-rate ANC system, a dynamic matching algorithm is added to the ANC process, which is responsible for acquiring $x_h(n)$, $u_h(n)$, and $e_h(n)$ at specific time intervals. The intervals can be preset before the control starts; for example,

they can be set to 1000 times the period of the low sampling rate or adjusted in the control state. The mirror noise portion of $u_h(n)$ and the aliasing noise portion of $x_h(n)$ and $e_h(n)$ are estimated in the regions with the high sampling rate, and then appropriate values of $T_{xd}(z)$, $T_{ud}(z)$, and $T_{ed}(z)$ are selected from the constructed digital filter library to achieve adaptation. As $G(z)$ may change with the variations in digital reconstruction and anti-aliasing filters, the dynamic matching algorithm needs to simultaneously adapt to $\hat{G}(z)$ to ensure the correct operation of the adaptive ANC algorithm in regions with a low sampling rate.

Considering the circuit components in the regions with a low sampling rate, the secondary path transfer function of the system is

$$G(z) = T_{ed}(z) \mathcal{Z} \left\{ \mathcal{L}^{-1} [C_e(s) T_{ea}(s) G_p(s) T_{ua}(s) C_u(s)] \right\} T_{ud}(z) \tag{3}$$

where \mathcal{L}^{-1} denotes the inverse Laplace transform, and \mathcal{Z} denotes the z-transform. The true transfer function from $u_h(n)$ to $e_h(n)$ via the loudspeaker is $G_h(z)$, and we let $\hat{G}_h(z)$ be the estimate of $G_h(z)$. Each time the digital reconstruction and anti-aliasing filters are updated, a new estimate of the secondary path transfer function can be obtained according to

$$\hat{G}(z) = T_{ed}(z) \hat{G}_h(z) T_{ud}(z) \tag{4}$$

Therefore, during the identification phase, the values of $\hat{G}_h(z)$ corresponding to each filter group can be calculated in advance after the identification of $G_h(z)$ is completed.

3.1. Construction of a Digital Filter Library in Regions with a High Sampling Rate

The adaptation of digital reconstruction and anti-aliasing filters can be implemented with online design methods or library-based methods. Online design methods dynamically calculate the filter parameters during the control process, while library-based methods set a library composed of a large number of filters before the control starts. In order to simplify the filter-matching process and ensure the stable operation of the filters, this study adopts a library-based method. Before the control starts, a large number of filters are arranged to form a filter library. In the control process, only the most suitable filters need to be selected from the filter library, with no need for online filter design. First, $T_{xd}(z)$, $T_{ud}(z)$, and $T_{ed}(z)$ are designed. These transfer functions have the following general form:

$$H(z) = \frac{Y(z)}{X(z)} = \frac{\sum_{k=0}^q b_k z^{-k}}{1 + \sum_{k=1}^p a_k z^{-k}} \tag{5}$$

where $\{b_k\}$ and $\{a_k\}$ are filter coefficients that determine the locations of the zeros and poles of $H(z)$, respectively, $X(z)$ is the z-transform of the input signal, and $Y(z)$ is the z-transform of the output signal. Different FIR filters or IIR filters can be implemented based on different values of $\{a_k\}$ and $\{b_k\}$. Regardless of whether one is using an FIR filter or IIR filter, one can refer to mature filter models such as the Butterworth, Chebyshev, Elliptics, and Bessel models when constructing the filter library. Chebyshev-I low-pass filters exhibit equal ripples in the passband, fast attenuation in the transition band, and a monotonic decrease attenuation with the frequency in the stopband. The squared amplitude response of the Nth-order analog Chebyshev filter is

$$|H_a(\Omega)|^2 = \frac{1}{1 + \varepsilon^2 T_N^2\left(\frac{\Omega}{\Omega_p}\right)} \tag{6}$$

where Ω_p denotes the passband cut-off frequency of the analog filter, ϵ is a parameter that determines the size of the ripples within the passband, and $T_N(x)$ is the first type of Chebyshev polynomial [33]:

$$T_N(x) = \begin{cases} \cos(N \arccos x) & |x| \leq 1 \\ \cosh(N \operatorname{arccosh} x) & |x| > 1 \end{cases} \quad (7)$$

Selecting different values of Ω_p , ϵ , and N , we obtain the constant H_0 and poles p_k . Then, the following transfer function of the analog filter can be obtained:

$$H_a(s) = \frac{H_0}{\prod_k (s - p_k)} \quad (8)$$

After the completion of the analog filter design, the corresponding digital Chebyshev-I-type low-pass filter can be constructed with such methods as bilinear transformation:

$$H(z) = H_a(s) \Big|_{s=\frac{z-1}{z+1}} = \frac{H_0}{\prod_k \left(\frac{z-1}{z+1} - p_k \right)} \quad (9)$$

After sorting, Equation (9) is transformed into the form shown in Equation (5), thus yielding the filter output

$$y(n) = \sum_{k=0}^q b_k x(n-k) - \sum_{k=1}^p a_k y(n-k) \quad (10)$$

and the actual frequency response of the digital filter

$$H(e^{j\omega}) = H(z) \Big|_{z=e^{j\omega}} = \frac{\sum_{k=0}^q b_k e^{-j\omega k}}{1 + \sum_{k=1}^p a_k e^{-j\omega k}} = |H(e^{j\omega})| e^{j\varphi(\omega)} \quad (11)$$

where ω is the radian frequency, $|H(e^{j\omega})|$ is the amplitude response of digital filter $H(z)$, and $\varphi(\omega)$ is the phase response of $H(z)$. Then, the group delay response of the filter is

$$\tau(\omega) = -\frac{d\varphi(\omega)}{d\omega} \quad (12)$$

For the first, second, third, and fourth orders of Chebyshev-I-type filters, assuming that the high sampling rate is 40 kHz and the cut-off frequency of the passband is 2200 Hz, we can derive the amplitude response and group delay curves, as shown in Figure 3.

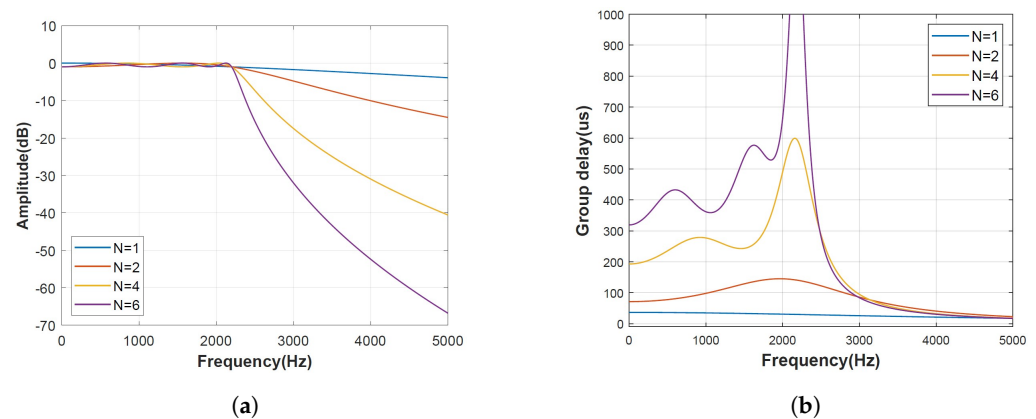


Figure 3. Frequency response and group delay curves of Chebyshev-I-type filters with different orders: (a) amplitude response; (b) group delay.

When constructing a digital filter library, the stored content includes the filter coefficients corresponding to different filter groups $T_{xd}(z)$, $T_{ud}(z)$, and $T_{ed}(z)$ and the squares of the amplitudes of the frequency responses $|T_{xd}(\omega)|^2$, $|T_{ud}(\omega)|^2$, and $|T_{ed}(\omega)|^2$. The average group delays within the control band from ω_1 to ω_2 are calculated with

$$\tau = \frac{1}{\omega_2 - \omega_1} \int_{\omega_1}^{\omega_2} \tau(\omega) \quad (13)$$

with $(\tau_{xd}$, τ_{ud} , and $\tau_{ed})$ and $\hat{G}(z)$. The storage of these data as the frequency response, group delay, and $\hat{G}(z)$ when constructing a filter library is beneficial for reducing the computational cost of dynamic filter adaptation in the ANC process.

In addition to Chebyshev-I-type low-pass filters, other models can also be used to construct digital filters with different features. In addition, we can also use the impulse response invariance method to convert IIR filters into FIR filters. As digital filter libraries are constructed offline, filter design tools can be used in filter design and optimization.

3.2. Data-Driven Dynamic Matching of Reconstruction Filters

The negative impacts of the mirror noise comprise two aspects: (1) the signal output of the reconstruction filter propagates directly to the human ear via the power amplifier and loudspeaker, directly affecting the listener's experience; (2) after the reconstructed mirror noise is propagated through the sound field, it is picked up again by the error microphone and reference microphone, which may introduce more aliasing noise. Therefore, the dynamic matching of the reconstruction filter is extremely important. During the control process, a set of reference signal data and error signal data with a high sampling rate are cached after certain periods of time for power spectrum estimation. The calculation formula is

$$\begin{aligned} \hat{S}_{xx,k}(m) &= \lambda \hat{S}_{xx,k}(m-1) + (1-\lambda) |X_{h,k}(m)|^2 \\ \hat{S}_{ee,k}(m) &= \lambda \hat{S}_{ee,k}(m-1) + (1-\lambda) |E_{h,k}(m)|^2 \\ \hat{S}_{uu,k}(m) &= \lambda \hat{S}_{uu,k}(m-1) + (1-\lambda) |U_{h,k}(m)|^2 \end{aligned} \quad (14)$$

where λ is the forgetting factor; and $X_{h,k}(m)$, $E_{h,k}(m)$, and $U_{h,k}(m)$ represent the spectra at the k th frequency point of $x_h(n)$, $e_h(n)$, and $u_h(n)$ in the m th iteration, respectively. The estimated power spectral density of the mirror noise introduced at the position of the error microphone $u_h(n)$ is

$$\hat{S}_{ue,k}(m) = |\hat{S}_{se_{h,k}}(m)|^2 \hat{S}_{uu,k}(m) \quad (15)$$

where $\hat{S}_{se_{h,k}}(m)$ denotes the high-sampling-rate-based estimate of the transfer function from the loudspeaker to the error microphone.

Next, we set the allowed upper limit of the power spectral density (PSD) of the mirror noise. In order to improve the comfort of an active noise control system such as an active headrest, it is necessary to consider the impact of mirror noise on the control system in different scenarios: (1) when the high-frequency noise contained in the sound source is easily heard, it is only required that the magnitude of mirror noise should not exceed that of the primary sound source; (2) when the high-frequency noise of the primary sound source is hardly heard, it is necessary to improve the high-frequency sensation brought by the mirror noise. Hence, for the frequency coefficient $k > \frac{k_L}{2}$, where k_L is the frequency coefficient corresponding to the low sampling rate, the following constraints are set:

$$\begin{cases} |T_{ud}(k)|^2 \hat{S}_{ue,k}(m) \leq C_1(k) \hat{S}_{ee,k}(m), & |A(k)|^2 \hat{S}_{ee,k}(m) > P_{t,k}(m) \\ |A(k)|^2 |T_{ud}(k)|^2 \hat{S}_{ue,k}(m) \leq P_{t,k}(m), & |A(k)|^2 \hat{S}_{ee,k}(m) \leq P_{t,k}(m) \end{cases} \quad (16)$$

where $C_1(k)$ denotes the power spectral ratio of the specified mirror noise with respect to the actually received mirror noise, and $P_{t,k}(m)$ denotes multiplication of the maximum value of $\hat{S}_{ee,k}(m)$ (where $0 < k < \frac{k_L}{2}$) when weighted by the equal-response curve $A(k)$ [20]. If the primary sound source has weak high-frequency content, the upper limit of the allowed

power spectrum of the mirror noise is given by $P_{t,k}(m)$. However, if the proportion of the high-frequency components is significant, then the upper limit is decided by $C_1(k)\hat{S}_{ee,k}(m)$.

$$P_{t,k}(m) = C_2(k) \cdot \max_{0 < k < \frac{k_L}{2}} \left[|A(k)|^2 \hat{S}_{ee,k}(m) \right], \quad k > \frac{k_L}{2} \tag{17}$$

where $C_2(k)$ denotes the margin coefficient preset before the ANC starts.

Finally, the group delays τ_{ud} are compared for the meeting of the filter groups in Equation (16) in the digital filter library, and the filter group with the smallest average group delay in the control frequency band is selected as the reconstruction filter in this study.

3.3. Dynamic Matching of Data-Driven Anti-Aliasing Filters

During the control process, the power spectrum of the output signal of each individual filter can be estimated based on the amplitude–frequency response of the filter.

$$\begin{aligned} \hat{S}_{xx,k,p}(m) &= \left| T_{xd,p}(k) \right|^2 \hat{S}_{xx,k}(m) \\ \hat{S}_{ee,k,p}(m) &= \left| T_{ed,p}(k) \right|^2 \hat{S}_{ee,k}(m) \end{aligned} \tag{18}$$

where p is the selected filter number in the filter library. Assuming that the extraction ratio of the high sampling rate over the low sampling rate is Q , in the digital extraction process, the reference signal and error signal introduce the following aliasing noise in the frequency coefficient range of $0 < k < \frac{k_L}{2}$:

$$\begin{aligned} N_{xx,k,p}(m) &= \sum_{i=1}^{Q-1} \left| T_{xd,p}(ik_L + k) \right|^2 \hat{S}_{xx,ik_L+k,p}(m) + \sum_{i=1}^Q \left| T_{xd,p}(ik_L - k) \right|^2 \hat{S}_{xx,ik_L-k,p}(m) \\ N_{ee,k,p}(m) &= \sum_{i=1}^{Q-1} \left| T_{ed,p}(ik_L + k) \right|^2 \hat{S}_{ee,ik_L+k,p}(m) + \sum_{i=1}^Q \left| T_{ed,p}(ik_L - k) \right|^2 \hat{S}_{ee,ik_L-k,p}(m) \end{aligned} \tag{19}$$

For the reference microphone and error microphone, the coherence between the aliasing noise and original low-frequency noise has different impacts on the control system [1]. When the aliasing noise is uncorrelated with the original low-frequency noise, the control system often suppresses the aliasing of the reference microphone more strictly. According to Equations (18) and (19), once the filter is selected, the dynamic ranges of the reference microphone and the error microphone in the control frequency band can be calculated in advance, satisfying the following conditions:

$$\begin{aligned} D_{x,k}(m) &= 10 \log_{10} \frac{\hat{S}_{xx,k,p}(m)}{N_{xx,k,p}(m)} \\ D_{e,k}(m) &= 10 \log_{10} \frac{\hat{S}_{ee,k,p}(m)}{N_{ee,k,p}(m)} \end{aligned} \tag{20}$$

According to the preset constraints over the dynamic ranges of $D_{x,k}(m) \geq D_{x,k,\min}$ and $D_{e,k}(m) \geq D_{e,k,\min}$, the digital anti-aliasing filter groups that meet these requirements can be selected. Finally, comparing the group delays of the selected filter groups in the digital filter library, the filter group with the smallest average group delay in the control frequency band is selected as the digital anti-aliasing filter employed in this study.

3.4. Analysis of Computational Complexity

The computational complexity is jointly determined by the extraction ratio Q , the filter order N_h , the period of dynamic matching, and the number of Fourier transform points. Let $Q = 8$ and $N_h = 6$; $\hat{G}(z)$ and $W(z)$ have 256 orders. Each of the filter libraries for $T_{xd}(z)$, $T_{ud}(z)$, and $T_{ed}(z)$ is composed of 20 filters. In the process of power spectrum estimation, a 1024-point Fourier transform is employed. Considering the acoustic feedback of the secondary path, the average numbers of multiplication operations with different channel numbers are shown in Table 1 for a comparison with the single-rate method. The order of the FIR filter selected in Bai’s method is 40, while sixth-order direct Type I IIR

filters are selected in this study. The update period of the secondary path is 1000 times for the period with the low sampling rate.

Table 1. Average number of multiplication operations compared with the single-rate method.

Reference Microphones	Secondary Sources	Error Microphones	Single-Rate Method	Bai's Method	Dynamic Matching Method
1	1	1	100%	112%	127%
1	2	1	200%	216%	236%
2	2	1	400%	420%	444%
2	2	2	600%	624%	654%
4	4	2	2400%	2440%	2490%

As the process of the dynamic matching algorithm is only required at long intervals, the amount of computation introduced in each sampling interval is limited. In the case with one reference microphone, one secondary sound source, and one error microphone, the multiplication operations of Bai's method and the dynamic matching method compared with single-rate methods are increased by 12% and 27%, respectively. As the number of channels increases, the proportion of the increase multiplications continuously decreases. In the case with two reference microphones, two secondary sound sources, and two error microphones, the increased multiplication operations of Bai's method and the proposed method are about 4% and 9%. In practical applications, virtual microphone technology [34,35] is often used in low-sampling-rate regions, so the proportion of computational complexity introduced by the proposed method will be further reduced.

4. Experimental Validation

4.1. Experimental Setup

A laboratory experimental system was set up in an anechoic chamber whose inside space had dimensions of 6.54 m × 4.84 m × 4.74 m. The free-field radius of the anechoic chamber was 1.1 m, and the background noise was 12.1 dBA, as shown in Figure 4. In the anechoic chamber, a loudspeaker serving as the primary sound source, a reference microphone, an error microphone, a monitoring microphone, and an active headrest were arranged. Figure 5 shows a flowchart of the experimental system. The embedded real-time processor for ANC was mainly composed of an XC7K325T FPGA produced by the Xilinx Company (San Jose, CA, USA) and a TMS320C6678 digital signal processor (DSP) produced by the TI company (Dallas, TX, USA). The FPGA was responsible for data acquisition and interface management, while the DSP performed algorithm calculations. The core processor of the embedded real-time processor for monitoring was an XC7Z020 system on chip (SOC). The type of analog-to-digital converter (ADC) used was AD7606B, and the digital-to-analog converter (DAC) used was LTC2755-16; the quantization bits of both the ADC and DAC chips were 16 bits. The conditioning circuits provided a constant current source of 4 mA for the microphones, the type of microphones was YG-201, and the type of speaker was Swan-B4N. The power amplifiers used were CA8000C models produced by Harman (Stamford, CT, USA), and the DSP debugger was TL-XDS560V2.

All of the ANC signal-processing tasks were implemented with embedded real-time processors, and the computer was only used to control the working status of the DSP and to receive the network data from the monitoring microphone. The monitoring microphone, which was in close proximity to the error microphone, was only used to monitor the effect of noise reduction and did not participate in the control process. The embedded real-time processor for monitoring received the monitored microphone data from the ADC and then sent data to the computer through a network cable. In the experimental process, the high sampling rate was set to 40 kHz, and the low sampling rate was set to 5 kHz.

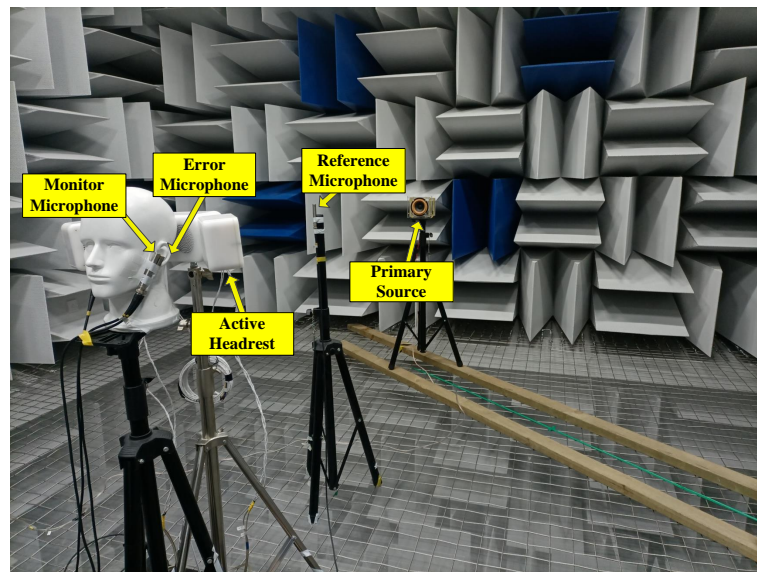


Figure 4. Experimental system in an anechoic chamber.

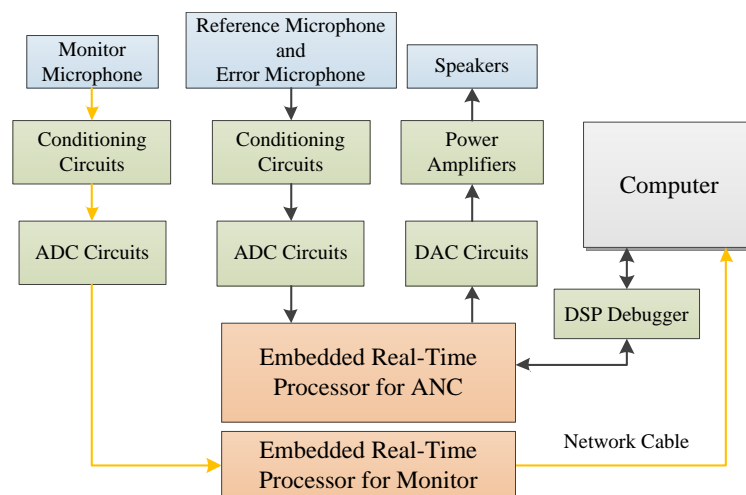


Figure 5. Flowchart of the experimental process.

This experiment aimed to test the effect of the proposed method in improving the noise reduction performance by changing the direction of incoming waves from primary sound sources with different spectral structures. For convenience when comparing the noise reduction performance of the proposed method and other methods, the primary sound source was arranged at multiple test locations during the experiment, and the top view of the experimental system's layout is shown in Figure 6.

The location of the error microphone was taken as the origin; the direction pointing towards the reference microphone was the $y+$ direction; the direction perpendicular to the y -axis and pointing to the right was the $x+$ direction. The reference microphone was mounted at the $(0, 100)$ coordinates; d_1 and d_2 denote the distances from the primary sound source to the reference microphone and to the error microphone, respectively; and θ denotes the angle between the straight line connecting the error microphone with the primary sound source and the y -axis. The noise reduction effect produced by the active headrest at the position of the monitoring microphone was measured for different locations and input signals of the primary sound source. In the practical use of headrests, error microphones are set around the head, and the real sound sources in the ears are estimated with physical microphones. As the aim of the experiment was to compare the proposed method with traditional methods, the error microphone was placed directly on the left

ear in order to reduce the interference with other factors, and only the control effect at the position of the left ear of an artificial head was tested in the experiment.

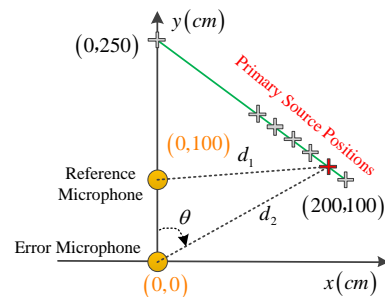


Figure 6. Top view of the layout of the experimental system.

4.2. Experimental Process and Results

Four types of primary sound sources were used in the experiment. The first type (marked “type a”) was band-limited white noise, with the highest frequency being below 500 Hz; the second (marked “type b”) and the third (marked “type c”) were also white noise, but with the highest frequencies being 2000 Hz and 5000 Hz, respectively. The last type of primary noise, “type d”, was a special primary noise that we constructed; the frequency components from 2000 Hz to 5000 Hz were raised unequally, and the frequency components below 2000 Hz were weakened unequally. The acoustic power levels emitted by the primary sound source of these four types were about 84 dB, 91 dB, 95 dB, and 93 dB, respectively. The whole ANC process included two stages: the offline identification stage and the ANC stage. In the identification stage, the primary sound was muted, $\hat{G}_h(z)$ from Equation (4) was obtained, and $\hat{G}(z)$ was calculated and stored in the library, together with the filter coefficients and τ , as described in Section 3. In the control stage, different types of primary sound sources were played in turn, setting the $u(n)$ value shown in Figure 1 to 0, and we obtained the ANC off-spectrum density of the monitor microphone. Then, by changing the program in the DSP, we obtained different noise reduction results.

When the primary sound source was located at point (192, 106), the noise reduction effects of different methods were determined, as demonstrated in Figure 7 for different types of primary sound sources. The noise reduction areas are outlined with green dashed lines, and the areas with obvious mirror noise are outlined with red dashed lines. The large θ values at this position led to small values of $(d_2 - d_1)$. Except for a slight noise reduction effect on the primary sound source below 500 Hz, all three methods had no significant noise reduction effects on the other three types of primary sound sources. Meanwhile, severe mirror noise was generated by Bai’s method, as shown in Figure 7b, and a significant uplift occurred from 1200 Hz to 2200 Hz, as shown in Figure 7d.

As θ continued to decrease, the value of $(d_2 - d_1)$ increased, so the three methods all demonstrated continuously improved noise reduction effects. When the primary sound source was located at point (112, 166), the noise reduction effects of different methods were determined for different types of primary sound sources, as shown in Figure 8. The single-rate method had poor noise reduction effects, while Bai’s method and the method proposed in this study showed significant noise reduction effects, as shown in Figure 8a,b. As shown in Figure 8c, the proposed method gave superior results to those of the other two methods. It is noted that the results of Bai’s method suffered from severe mirror noise, as shown in Figure 8a,b, and a significant uplift occurred from 500 Hz to 2500 Hz, as shown in Figure 8d.

With a further decrease in θ , the noise reduction effect of the single-rate method began to increase regardless of the spectra of the primary sound source. When the primary sound source was located at point (0, 250), the noise reduction effects of different methods for different types of primary sound sources were determined, as shown in Figure 9. In this case, the three methods achieved good noise reduction effects in the low-frequency parts shown in Figure 9a,b, while the result given by Bai’s method still suffered from severe

mirror noise. As shown in Figure 9c, the noise reduction effect of Bai’s method on the primary sound source did not continue to increase with the decrease in θ , and, as shown in Figure 9d, it still brought a serious noise uplift, as shown in the results.

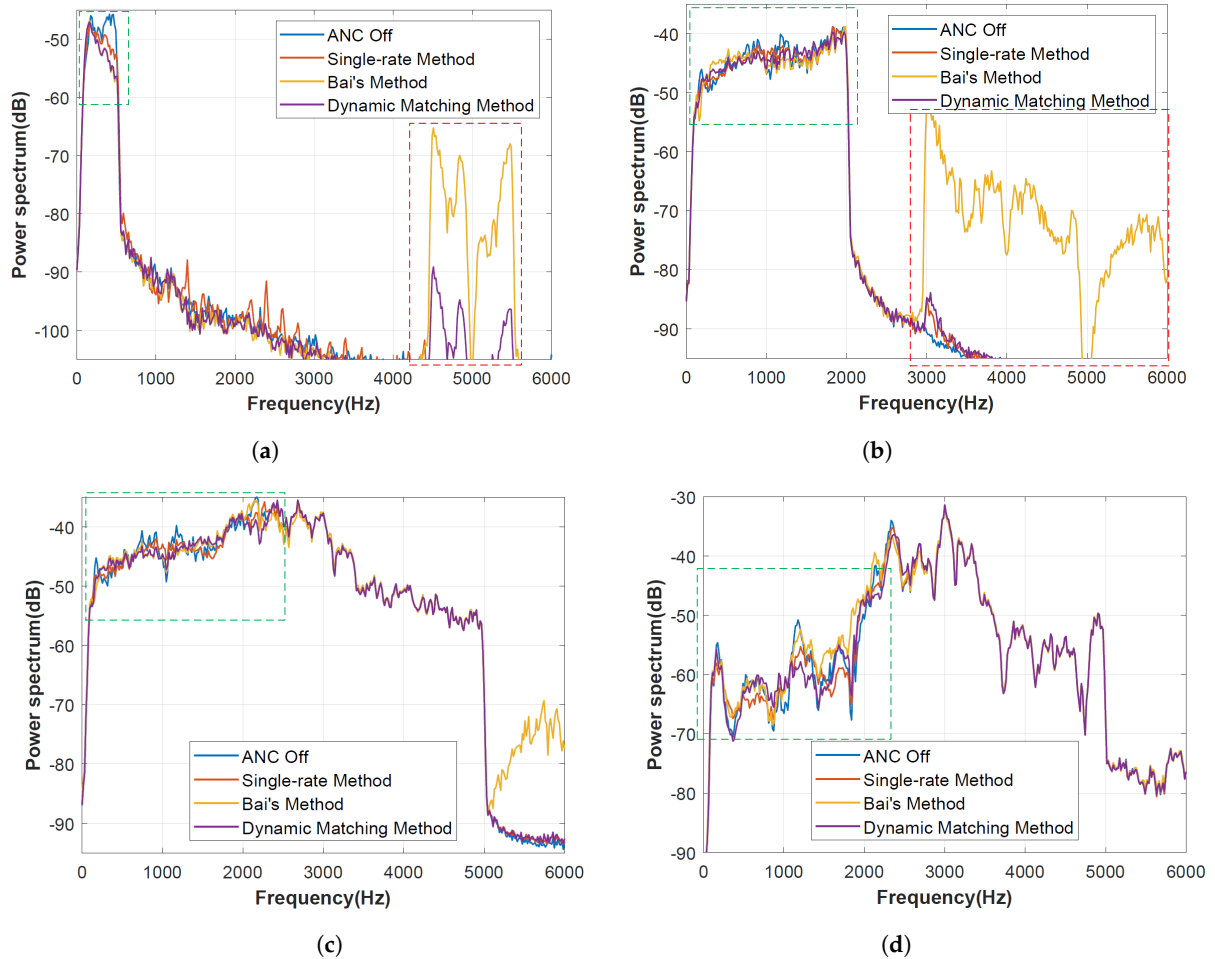


Figure 7. Power spectra of the residual noise at the location of the monitoring microphone when the primary sound source was located at the point (192, 106): (a) the spectrum of the primary sound source was distributed below 500 Hz; (b) the spectrum of the primary sound source was distributed below 2000 Hz; (c) the spectrum of the primary sound source was relatively uniformly distributed below 5000 Hz; (d) the spectrum of the primary sound source was distributed below 5000 Hz with a larger amplitude in the range of 2500–3500 Hz.

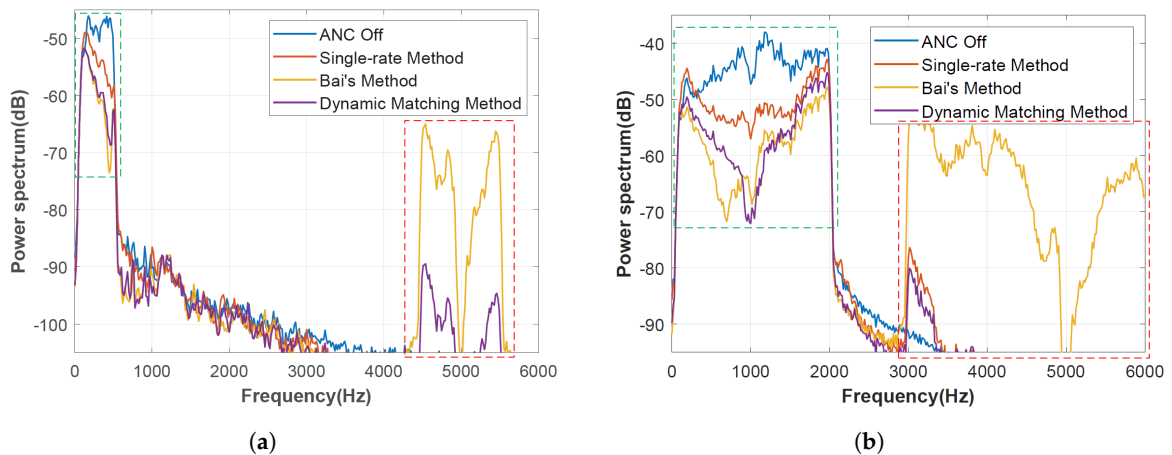
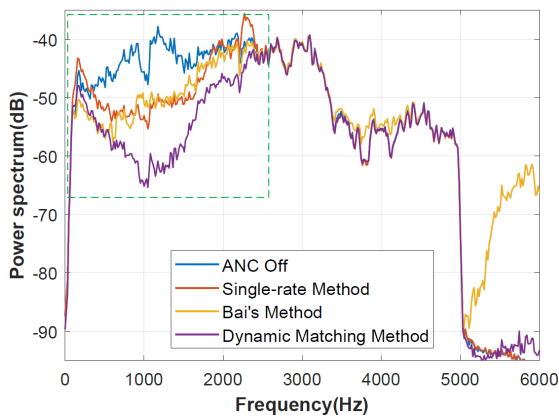
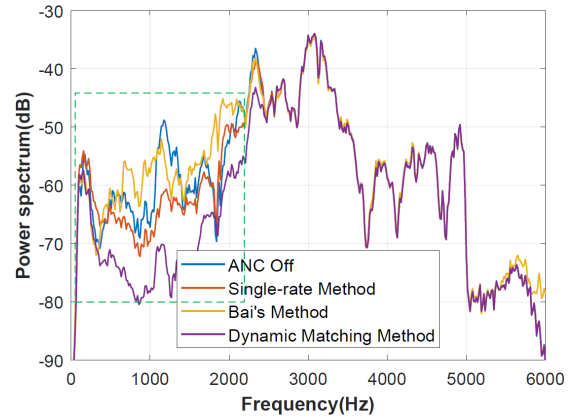


Figure 8. Cont.

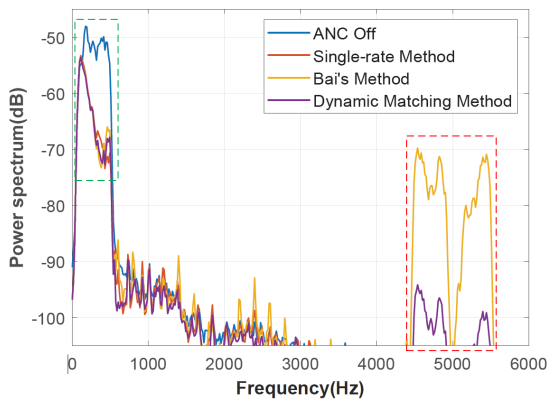


(c)

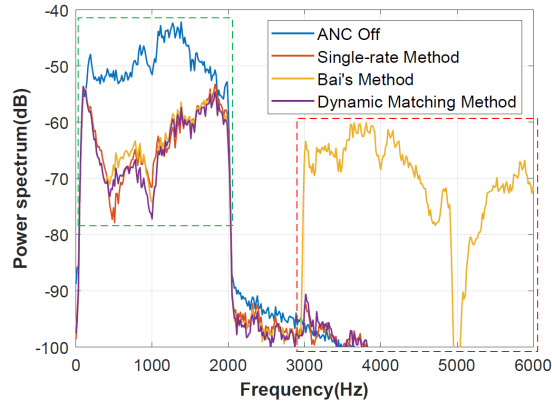


(d)

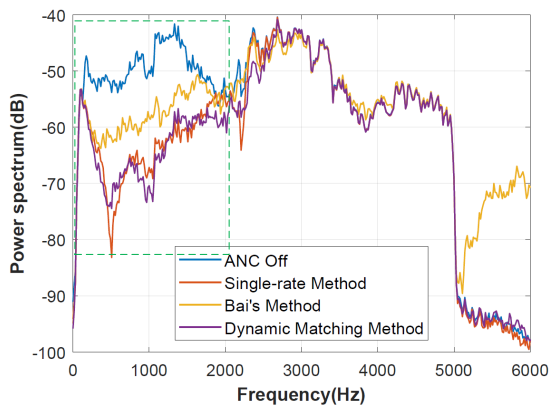
Figure 8. Power spectra of the residual noise at the location of the monitoring microphone when the primary sound source was located at the point (112, 166): (a) the spectrum of the primary sound source was distributed below 500 Hz; (b) the spectrum of the primary sound source was distributed below 2000 Hz; (c) the spectrum of the primary sound source was relatively uniformly distributed below 5000 Hz; (d) the spectrum of the primary sound source was distributed below 5000 Hz with a larger amplitude in the range of 2500–3500 Hz.



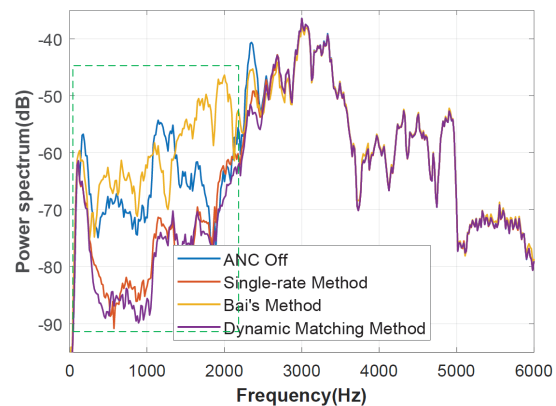
(a)



(b)



(c)



(d)

Figure 9. Power spectra of the residual noise at the location of the monitoring microphone when the primary sound source was located at point (0, 250): (a) the spectrum of the primary sound source was distributed below 500 Hz; (b) the spectrum of the primary sound source was distributed below 2000 Hz; (c) the spectrum of the primary sound source was relatively uniformly distributed below 5000 Hz; (d) the spectrum of the primary sound source was distributed below 5000 Hz with a larger amplitude in the range of 2500–3500 Hz.

4.3. Discussion of the Experimental Results

According to the experimental results in Figures 7–9, one can see that both the value of θ and the spectrum of primary noise affect the performance of an adaptive ANC system. We define the average noise reduction (ANR) as the average of the difference in power spectra between ANC Off and ANC On within a specified frequency range. The ANR values for different positions and methods are displayed in Table 2.

Table 2. Comparison of ANR values for different positions and methods.

Position (cm)	Method	ANR for “type a” (100 Hz–500 Hz) (dB)	ANR for “type b” (100 Hz–2000 Hz) (dB)	ANR for “type c” (100 Hz–2000 Hz) (dB)	ANR for “type d” (100 Hz–2000 Hz) (dB)
(192, 106)	Single-Rate Method	2.1	0.2	0.2	0.2
(192, 106)	Bai’s Method	3.5	0.5	0.0	−2.0
(192, 106)	Dynamic Matching Method	3.5	0.2	0.1	0.0
(112, 166)	Single-Rate Method	5.6	6.5	5.4	2.3
(112, 166)	Bai’s Method	12.2	14.2	6.4	−2.5
(112, 166)	Dynamic Matching Method	10.9	12.4	12.1	10.8
(0, 250)	Single-Rate Method	12.8	13.8	13.6	11.2
(0, 250)	Bai’s Method	13.0	13.2	7.8	−5.3
(0, 250)	Dynamic Matching Method	13.2	14.6	14.3	12.6

For “type a” and “type b” primary noise, the spectrum distribution was within half of the sampling rate but the bandwidths were different. Bai’s method had the best ANRs at (192, 106) and (112, 166) within the ranges of 100 Hz–500 Hz and 100 Hz–2000 Hz, respectively, but the mirror noise caused by Bai’s method was above −66 dB and −52 dB, respectively, which would directly affect the listener’s experience. The ANR values of the proposed method were slightly lower than those of Bai’s method at positions (192, 106) and (112, 166), but they were much better than those of the single-rate method, and the mirror noise was under −89 dB and −80 dB, respectively, which meant that the group delay was better compromised with the mirror noise cancellation.

For “type c” and “type d” primary noise, there were components above half of the sampling rate, but the ratios of components above and below the sampling rate were different. The aliasing noise is an important factor in ANC systems. The ANR values of Bai’s method decreased by more than 5 dB in comparison with that of “type b” in positions (112, 166) and (0, 250). The proposed method had better anti-aliasing noise reduction properties than those of Bai’s method as the ANR values at position (0, 250) were at least 6.5 dB better. At the same time, the proposed method had better space robustness than that of the single-rate method as the ANR values in position (112, 166) were better than 6.7 dB and 8.5 dB, respectively, meaning that the group delay was better compromised with the aliasing noise cancellation.

The experimental results fully demonstrate that the proposed method for dynamic matching of reconstruction and anti-aliasing filters can effectively improve the spatial robustness of a system while controlling the mirror noise and aliasing noise.

5. Conclusions

A dynamic matching method was proposed for the design of reconstruction and anti-aliasing filters in order to address the problems associated with group delay and high-frequency noise in systems with fixed reconstruction and anti-aliasing filters. The mirror noise and anti-aliasing noise evaluated in the digital regions at a high sampling rate are used to achieve the matching of digital reconstruction and anti-aliasing filters at a low sampling rate. Active noise control experiments were conducted in an anechoic chamber for primary sound sources with different spectral structures and different directions of incoming sound waves, and the experimental results demonstrated the following:

- (1) The reconstruction filter directly affected the mirror noise exported by the ANC system, and primary sound sources with different spectral structures had different requirements for the attenuation characteristics of the reconstruction filter;
- (2) For primary sound sources with weak low-frequency components, anti-aliasing filters with slow roll-off rate can be used; however, when high-frequency components become significant, such anti-aliasing filters may limit the noise reduction of ANC and even cause low-frequency uplift;
- (3) Increasing the roll-off rate of reconstruction and anti-aliasing filters is often not the best choice as these two types of filters will bring additional group delays to the system; therefore, one needs to consider a trade-off between the suppression of high-frequency noise and the group delay for practical systems;
- (4) The proposed method can significantly improve the noise reduction performance of the ANC system while effectively suppressing the mirror noise and aliasing noise.

Future research will extend these results to the typical ANC applications mentioned in the introduction, especially for the scenes with directional primary sources. Furthermore, an investigation into the effect of methods combining the proposed method and beamforming technology in an ANC system will be conducted.

Author Contributions: Conceptualization, F.Z. and X.L.; Data curation, F.Z., Y.W. (Yanqin Wu), and Y.W. (Yifan Wang); Formal analysis, F.Z.; Funding acquisition, X.L.; Methodology, F.Z.; Project administration, X.L.; Resources, X.L.; Software, F.Z.; Supervision, Y.W. (Yanqin Wu); Validation, Y.W. (Yanqin Wu) and Y.W. (Yifan Wang); Visualization, F.Z.; Writing—original draft, F.Z.; Writing—review and editing, Y.W. (Yanqin Wu), Y.W. (Yifan Wang), and X.L. All authors have read and agreed to the published version of the manuscript. All authors will be informed about each step of manuscript processing, including submission, revision, revision reminders, etc., via emails from our system or assigned Assistant Editor.

Funding: This research was funded by National Key R&D Program of China under Grant 2023QY0803.

Institutional Review Board Statement: This study was conducted according to the guidelines of the Declaration of Helsinki and approved by the Institutional Review Board of the Key Laboratory of Noise and Vibration Research, Institute of Acoustics, Chinese Academy of Sciences (NV2021-0502).

Informed Consent Statement: Informed consent was obtained from all subjects involved in the study.

Data Availability Statement: The data presented in this study are available upon request from the corresponding author.

Conflicts of Interest: The authors declare no conflicts of interest.

References

1. Elliott, S.J. *Signal Processing for Active Control*; Elsevier: Amsterdam, The Netherlands, 2000.
2. Lu, L.; Yin, K.L.; Lamare, R.C.; Zheng Z.; Yu, Y.; Yang, X.; Chen, B. A survey on active noise control in the past decade-Part I: Linear systems. *Signal Process.* **2021**, *183*, 108039. [[CrossRef](#)]
3. Siswanto, A.; Chang, C.Y.; Kuo, S.M. Active noise control for headrests. In Proceedings of the 2015 Asia-Pacific Signal and Information Processing Association Annual Summit and Conference (APSIPA), Hong Kong, China, 16–19 December 2015; pp. 688–692.
4. Chang, C.Y.; Chuang, C.T.; Kuo, S.M.; Lin, C.H. Multi-functional active noise control system on headrest of airplane seat. *Mech. Syst. Signal Process.* **2022**, *167*, 108552. [[CrossRef](#)]
5. Jung, W.; Elliott, S.J.; Cheer, J. Local active control of road noise inside a vehicle. *Mech. Syst. Signal Process.* **2019**, *121*, 144–157. [[CrossRef](#)]
6. Chen, W.; Xie, L.; Guo, J.; Liu, Z.; Li, X.; Lu, C. A computationally efficient feedforward time-frequency-domain hybrid active sound profiling algorithm for vehicle interior noise. *Mech. Syst. Signal Process.* **2023**, *194*, 110279. [[CrossRef](#)]
7. Chu, Y.J.; Mak, C.M.; Wu, M.; Wu, J.F.; Zhao, Y. A new variable spatial regularized FxLMS algorithm for diffusion active noise control. *Appl. Acoust.* **2023**, *211*, 109532. [[CrossRef](#)]
8. Ranjan, R.; He, H.; Murao, T.; Lam, B.; Woon-Seng, G. Selective active noise control system for open windows using sound classification. *Proc. INTER-NOISE NOISE-CON Congr.* **2016**, *253*, 1921–1931.
9. Luo, Z.; Shi, D.; Ji, J.; Shen, X.; Gan, W.S. Real-time implementation and explainable AI analysis of delayless CNN-based selective fixed-filter active noise control. *Mech. Syst. Signal Process.* **2024**, *214*, 111364. [[CrossRef](#)]

10. Shi, D.; Gan, W.S.; Lam, B.; Wen, S. Feedforward Selective Fixed-Filter Active Noise Control: Algorithm and Implementation. *IEEE/ACM Trans. Audio Speech Lang. Process.* **2020**, *28*, 1479–1492. [[CrossRef](#)]
11. Thi, J.; Morgan, D. Delayless subband active noise control. *IEEE Int. Conf. Acoust. Speech Signal Process.* **1993**, *1*, 181–184.
12. Morgan, D. An analysis of multiple correlation cancellation loops with a filter in the auxiliary path. *IEEE Trans. Acoust. Speech Signal Process.* **1980**, *28*, 454–467. [[CrossRef](#)]
13. Yang, F.; Wu, M.; Ji, P.; Yang, J. An Improved Multiband-Structured Subband Adaptive Filter Algorithm. *IEEE Signal Process. Lett.* **2012**, *19*, 647–650. [[CrossRef](#)]
14. Yang, F.; Enzner, G.; Yang, J. On the Convergence Behavior of Partitioned-Block Frequency-Domain Adaptive Filters. *IEEE Trans. Signal Process.* **2021**, *69*, 4906–4920. [[CrossRef](#)]
15. Nelson, P.; Hammond, J.; Elliott, S.J. Casual constraints on the active control of sound. In Proceedings of the ICASSP '87. IEEE International Conference on Acoustics, Speech, and Signal Processing, Dallas, TX, USA, 6–9 April 1987; pp. 145–148.
16. Elliott, S.J.; Rafaely, B. Frequency-domain adaptation of causal digital filters. *IEEE Trans. Signal Process.* **2000**, *48*, 1354–1364. [[CrossRef](#)] [[PubMed](#)]
17. Cheng-Yuan, C.; Sen, M.K. Complete parallel narrowband active noise control systems. *IEEE/ACM Trans. Audio Speech Lang. Process.* **2013**, *21*, 1976–1986.
18. Cheer, J.; Elliott, S.J. Comments on “Complete Parallel Narrowband Active Noise Control Systems”. *IEEE/ACM Trans. Audio Speech Lang. Process.* **2014**, *22*, 995–996. [[CrossRef](#)]
19. Elliott, S.J.; Jung, W.; Cheer, J. Causality and Robustness in the Remote Sensing of Acoustic Pressure, with Application to Local Active Sound Control. In Proceedings of the ICASSP 2019—2019 IEEE International Conference on Acoustics, Speech and Signal Processing (ICASSP), Brighton, UK, 12–17 May 2019; pp. 8484–8488.
20. Shen, X.; Shi, D.; Gan, W.S. A Wireless Reference Active Noise Control Headphone Using Coherence Based Selection Technique. In Proceedings of the ICASSP 2021—2021 IEEE International Conference on Acoustics, Speech and Signal Processing (ICASSP), Toronto, ON, Canada, 6–11 June 2021; pp. 7983–7987.
21. Williams, J.E.; Roebuck, I.F.J.; Ross, C.F. Anti-phase noise reduction. *Phys. Technol.* **1985**, *16*, 19–24. [[CrossRef](#)]
22. Kuo, S.M.; Morgan, D. *Active Noise Control Systems: Algorithms and DSP Implementations*; John Wiley & Sons, Inc.: Hoboken, NJ, USA, 1996.
23. Rabiner, L.R. *Feedback Control of Sound*; University of Southampton: Southampton, UK, 1997; pp. 1082–1103.
24. Bai, M.R.; Lin, Y.; Lai, J. Reduction of electronic delay in active noise systems—A multirate signal processing approach. *J. Acoust. Soc. Am.* **2002**, *111*, 916–924. [[CrossRef](#)] [[PubMed](#)]
25. Siswanto, A.; Chang, C.Y.; Kuo, S.M. Multirate Audio-Integrated Feedback Active Noise Control Systems Using Decimated-Band Adaptive Filters for Reducing Narrowband Noises. *Sensors* **2020**, *20*, 6693. [[CrossRef](#)]
26. Shi, D.; Gan, W.S.; He, J.; Lam, B. Practical implementation of multichannel filtered-x least mean square algorithm based on the multiple-parallel-branch with folding architecture for largescale active noise control. *IEEE Trans. Very Large Scale Integr. Syst.* **2020**, *28*, 940–953. [[CrossRef](#)]
27. Miyake, T.; Iwai, K.; Kajikawa, Y. Head-Mounted Multi-Channel Feedforward Active Noise Control System for Reducing Noise Arriving From Various Directions. *IEEE Access* **2023**, *29*, 6935–6943. [[CrossRef](#)]
28. Vered, Y.; Elliott, S. A Parallel Analog and Digital Adaptive Feedforward Controller for Active Noise Control. *IEEE/ACM Trans. Audio Speech Lang. Process.* **2024**, *32*, 1100–1108. [[CrossRef](#)]
29. Hashemian, R. Design of an active noise control system using combinations of dsp and fpgas. *PLD Conf. Proc.* **1995**, *10*, 21–26.
30. Kuo, S.M.; Panahi, I.; Chung, K.M.; Horner, T.; Nadeski, M.; Chyan, J. Design of active noise control systems with the tms320 family. *Tex. Instrum.* **1996**.
31. Vu, H.S.; Chen, K.H.; Sun, S.F.; Fong, T.M.; Hsu, C.W.; Wang, L. A power-efficient circuit design of feed-forward FxLMS active noise cancellation for in-ear headphones. In *VLSI Design, Automation and Test (VLSI-DAT)*; IEEE: Piscataway, NJ, USA, 2015; pp. 1–4.
32. Kim, Y.; Park, Y. Blockwise weighted least square active noise control for cpu-gpu architecture. *IEEE/ACM Trans. Audio Speech Lang. Process.* **2020**, *28*, 951–963. [[CrossRef](#)]
33. Rao, K.D.; Swamy, M.N.S. *Digital Signal Processing Theory and Practice*; Springer: Berlin/Heidelberg, Germany, 2018.
34. Jung, W.; Elliott, S.J.; Cheer, J. Estimation of the pressure at a listener’s ears in an active headrest system using the remote microphone technique. *J. Acoust. Soc. Am.* **2018**, *143*, 2858–2869. [[CrossRef](#)]
35. Zhang, J.; Zheng, C.; Zhang, F.; Li, X. A low complexity Volterra filtered error LMS algorithm with a Kronecker product decomposition. *Appl. Sci.* **2021**, *11*, 9637. [[CrossRef](#)]

Disclaimer/Publisher’s Note: The statements, opinions and data contained in all publications are solely those of the individual author(s) and contributor(s) and not of MDPI and/or the editor(s). MDPI and/or the editor(s) disclaim responsibility for any injury to people or property resulting from any ideas, methods, instructions or products referred to in the content.